

## Article

# Research on the Value of Rayleigh Damping Parameter in Explicit and Implicit Integrals for Dynamic Analysis of Large Structures

Yan Chen <sup>1,2</sup>, Haitao Wang <sup>1</sup>, Yougang Wang <sup>2</sup>, Junhong Zhang <sup>2</sup>, Zitong Bao <sup>2</sup>, Jianbo Li <sup>3,\*</sup>, Miaomiao Chen <sup>3</sup> and Peng Xu <sup>3</sup>

<sup>1</sup> Institute of Nuclear and New Energy Technology, Tsinghua University, Beijing 100084, China; yanchen@chinergy.com.cn (Y.C.); wanght@tsinghua.edu.cn (H.W.)

<sup>2</sup> China National Nuclear Corporation (CNNC), Beijing 100032, China; arcwyg@163.com (Y.W.); baozi9585@126.com (Z.B.)

<sup>3</sup> State Key Laboratory of Coastal and Offshore Engineering, Institute of Earthquake Engineering, School of Infrastructure Engineering, Dalian University of Technology, Dalian 116024, China; chenmiaomiao86@163.com (M.C.); 1325792990@mail.dlut.edu.cn (P.X.)

\* Correspondence: jianboli@dlut.edu.cn; Tel.: +86-18537083950

**Abstract:** Rayleigh damping is proportional to the combination of the structural mass matrix and stiffness matrix and is widely used in structural seismic analysis. The accuracy of seismic analysis of nuclear power structures directly depends on the value of the Rayleigh damping parameters. However, the stiffness component of Rayleigh damping is not included in the explicit integral, so the Rayleigh damping in the explicit and implicit integrals needs to be handled differently. LS-DYNA R11.1.0 software provides various calculation methods for the value of the Rayleigh damping parameter in the explicit integral. To investigate the influence of the value of the Rayleigh damping parameter in the explicit and implicit integrals on the results of the dynamic analysis of a nuclear power plant, the AP1000 nuclear island plant is taken as an example, and the explicit and implicit dynamic calculation are carried out respectively for the nuclear power plant, considering the soil–structure interaction. The results show that the Rayleigh damping parameter calculated by different methods in the explicit integral has a large influence on the results of seismic analysis of nuclear power plants. The mass component of Rayleigh damping in the explicit and implicit integrals takes the same value, and the stiffness component of Rayleigh damping in the explicit integrals is taken as the negative of the stiffness component in the implicit integrals. Thus, the results of the two dynamic analyses can be in good agreement. The results provide a reference for the application of Rayleigh damping in the explicit integral for the seismic analysis of nuclear power structures.

**Keywords:** nuclear power plants; rayleigh damping; soil–structure interaction; explicit and implicit integrals



**Citation:** Chen, Y.; Wang, H.; Wang, Y.; Zhang, J.; Bao, Z.; Li, J.; Chen, M.; Xu, P. Research on the Value of Rayleigh Damping Parameter in Explicit and Implicit Integrals for Dynamic Analysis of Large Structures. *Buildings* **2024**, *14*, 1286. <https://doi.org/10.3390/buildings14051286>

Academic Editor: Daniele Perrone

Received: 27 March 2024

Revised: 16 April 2024

Accepted: 29 April 2024

Published: 2 May 2024



**Copyright:** © 2024 by the authors. Licensee MDPI, Basel, Switzerland. This article is an open access article distributed under the terms and conditions of the Creative Commons Attribution (CC BY) license (<https://creativecommons.org/licenses/by/4.0/>).

## 1. Introduction

In the analysis of the soil–structure interactions of large-scale engineering structures, such as nuclear power and hydraulic engineering structures, damping consistently represents a difficult point in the research. Unlike the mass and stiffness in dynamic analysis, the physical meaning of damping is not yet clear [1] (friction within the structure, the filtering effect of the structure, the radiation damping effect of the soil, the influence of external damping, etc.). However, damping is an important factor in soil–structure interactions. Reasonable setting of the damping coefficient can make the simulation results more credible. On the contrary, unreasonable setting of the damping coefficient leads to serious error of calculation results that diverge from the real situation. The damping of soil is independent of frequency [2], but the damping ratio derived from Rayleigh damping shows that there is

a correlation between damping and frequency, which is obviously problematic. The safety and dynamic characteristics of special large-scale structures, such as hydraulic engineering and nuclear power plants, under earthquake action are a major issue and research topic with theoretical and practical significance.

Many domestic and foreign scholars have conducted research on how to determine the Rayleigh damping coefficient. Idriss et al. [1] used only the basic frequency of the structure to determine the damping coefficient. Yoshida et al. [3] proposed a method of calculating the damping coefficient within the main frequency range. Yu Ting et al. [4] comprehensively considered the spectral characteristics of seismic waves and the characteristics of the foundation soil layer and studied the selection method of the two control frequencies of the Rayleigh damping model. Wang Tianyou et al. [5] determined two mode shapes based on the basic frequency of the structure and the main characteristic frequency range of ground motion, and used them to calculate the damping coefficient. Lou Menglin et al. [6–8] used a proportional damping matrix modelling method based on the fundamental frequency of the structural system and the peak frequency of the seismic wave response spectrum. Pan Danguang et al. [9–11] used the error of the structural displacement response peak as the objective function, used the least squares method to determine the damping coefficient, and established an optimization equation for solving the Rayleigh damping coefficient. Cheng Ye et al. [12] established the optimization equation of the equivalent Rayleigh damping coefficient under hysteresis damping by taking the minimum acceleration response error of the site surface as the objective function. Yang et al. [13] proposed a method to calculate the Rayleigh damping coefficient based on the multi-modal weighted least squares method. Zhu Xiuyun et al. [14] discussed the differences between different calculation methods of the Rayleigh damping coefficient under nonlinear plant sites, and recommended the improved damping coefficient calculation method proposed by Zou Degao et al. [15]. Li Zhe et al. [16] discussed the impacts of different Rayleigh damping coefficients on the calculation results in the seismic response analysis of large quay cranes, and improved the damping coefficient calculation method and frequency selection method of the quay crane structure. Xu Zigang et al. [17] analyzed the dynamic response of a layered site under different earthquake motions and compared the time domain calculation results and the frequency domain equivalent linearization calculation results of the Rayleigh damping construction method commonly used in engineering, and based on the hysteretic damping ratio in frequency domain analysis, the Rayleigh damping coefficient in time domain analysis was constructed. Shi Youzhi et al. [18] took the shallow plain fill soil and silty clay in the Xiamen area as the research object and investigated the influence of the mass proportional damping coefficient  $\alpha$  and stiffness proportional damping coefficient  $\beta$  in Rayleigh damping on the response characteristics. Tang Yu et al. [19] believe that when the natural vibration characteristics of a high arch dam show long-period structural dynamic characteristics compared with the seismic wave spectrum distribution, the damping matrix model has a great influence on the calculation results. Haukaas, Terje [20] introduced the development of Rayleigh damping and modal damping options using updated tangent stiffness. Li, Sijia et al. [21] proposed an effective Rayleigh damping explicit/implicit transient analysis method that considered high-frequency filtering frictional contact. Jing, Zhang et al. [22] used a combination of on-site measurements and the finite element method to determine three damping coefficients, and obtained different damping coefficients. On the basis of idealizing the shear beam model, Huang, Jiandong et al. [23] proposed a more reasonable method for calculating the natural frequencies of different layers to determine the two coefficients of Rayleigh damping. Jiménez, Guillermo A. López et al. [24] studied the influence of Rayleigh damping parameters on soil pile structures and soil-wrapped platform structural systems in the presence of soft soil under seismic loads. Rahul, B. et al. [25] presented a simple and effective method for the determination of Rayleigh coefficients for a system with multiple degrees of freedom.

Other damping models have also been investigated by researchers. Valeriy et al. [26] assessed the dissipative properties of solids using a maximum resonance amplitude and a

minimum rate of vibration decay. Beytullah Temel [27] investigated the transient analysis of viscoelastic helical rods subject to time-dependent loads in the Laplace domain. Sherzod et al. [28] proposed a method to assess the dynamic characteristics of high-rise structures, taking into account the variability of slopes and the structure thickness in the framework of the one-dimensional theory of viscoelasticity. Temel et al. [29] studied free and forced vibration responses of viscoelastic parabolic arches of variable thicknesses. Noori et al. [30] presented an efficient numerical procedure for the solution of the dynamic response of functionally graded porous (FGP) beams.

Time history analysis is a common method for the seismic design of large structures. Cao et al. [31] proposed an optimal sensor placement approach for reconstructing full-field dynamic responses using a set of basic vectors obtained from high-fidelity data. Guo et al. [32] theoretically investigated the scattering characteristics of blasting stress waves, treated as elastic waves, at a linear interface crack in a deep rock mass with an even compressive in situ stress field. Deng et al. [33] presented an experimental–numerical investigation on an innovative fully prefabricated liftable connection for modular steel buildings.

The Rayleigh damping model is a commonly used damping model in time history analysis. Different values of the Rayleigh damping coefficient for explicit and implicit dynamic analysis will affect its calculation accuracy [34]. Selecting appropriate Rayleigh damping coefficients in explicit and implicit analysis is of great significance in order to accurately calculate the seismic response of nuclear power structures. However, there is currently limited research on the impact of the value of the Rayleigh damping coefficient on explicit integration, as well as how the Rayleigh damping coefficient should be taken in explicit and implicit integrations to ensure good consistency in the results. This article first introduces the calculation method of the Rayleigh damping coefficient in explicit and implicit analysis, applies different calculation methods of the Rayleigh damping coefficient to the seismic analysis of nuclear power structures, and studies its influence rules. This provides a parametric basis for the calculation of the Rayleigh damping coefficient in explicit and implicit dynamics analysis.

## 2. Rayleigh Damping

The real damping characteristics of typical structural systems are very complex and difficult to determine, and it is usually not necessary to express the damping of a typical viscous damping multi-degree-of-freedom system in the form of a damping matrix. Therefore, the array damping ratio with the same attenuation rate under self-vibration conditions is usually used to represent the damping of the actual structure.

Obviously, the simplest way to establish the damping matrix is to make it proportional to the mass matrix or stiffness matrix, since the undamped mode shapes are orthogonal to mass and stiffness. Therefore, the damping matrix can be expressed as:

$$[C] = a_0[M] \quad (1)$$

or:

$$[C] = a_1[K] \quad (2)$$

The units of the proportional constants  $a_0$  and  $a_1$  are  $s^{-1}$  and  $s$ , respectively, and the corresponding damping becomes mass proportional damping and stiffness proportional damping.

Relevant characteristics can be obtained by calculating the respective generalized mode damping values. The specific calculation process is as follows [35]:

$$[M]\{\ddot{u}\}_t + [K]\{\dot{u}\}_t + [C]\{u\}_t = -[M]\{\ddot{u}_g\}_t \quad (3)$$

$$\phi^T[M]\phi\{\ddot{u}\}_t + \phi^T[K]\phi\{\dot{u}\}_t + a_0\phi^T[M]\phi\{u\}_t = -\phi^T[M]\phi\{\ddot{u}_g\}_t \quad (4)$$

or:

$$\phi^T [M] \phi \{\ddot{u}\}_t + a_1 \phi^T [M] \phi \{\dot{u}\}_t + \phi^T [C] \phi \{u\}_t = -\phi^T [M] \phi \{\ddot{u}_g\}_t \quad (5)$$

Substituting into  $[C] = 2\zeta\omega[M]$  and (2) or (3) gives:

$$\zeta = \frac{a_0}{2\omega} \quad (6)$$

or:

$$\zeta = \frac{a_1\omega}{2} \quad (7)$$

Through Equations (6) and (7), it can be found that for mass ratio damping, the damping ratio is proportional to frequency. Mass damping (\*damping-part-mass) is used to weaken the low-frequency vibration of the structure, while for stiffness ratio damping, the damping ratio is inversely proportional to frequency. Stiffness damping (\*damping-part-stiffness) is used in the high-frequency mode of damping to reduce high-frequency oscillations in the response.

Usually only the main mode shapes are included in the uncoupled equations of motion, and the dynamic response usually includes contributions from all modes. Therefore, when the frequency range of the main mode shapes of a multi-degree-of-freedom system is very wide, the above two damping matrices will no longer be applicable, because inappropriate damping ratios will seriously distort the relative assignments of different modes.

A significant improvement can be obtained if one assumes that the damping is proportional to a combination of the mass and stiffness matrices. One combination is to add the two expressions in [36]:

$$[C] = \alpha[M] + \beta[K] \quad (8)$$

Equation (8) is the expression of Rayleigh damping, in which  $\alpha$  and  $\beta$  are the Rayleigh damping coefficients. From Equation (5), it can be seen that the accuracy of the structural seismic responses largely depends on the calculation of the Rayleigh damping coefficients in the dynamic time and history analysis. Thus, this paper focuses on the value of the Rayleigh damping parameter in explicit and implicit integrals for the dynamic analysis of large structures.

This kind of damping becomes Rayleigh damping. Through similar calculations, the relationship between damping ratio and frequency is as follows [36]:

$$\zeta_n = \frac{\alpha}{2\omega_n} + \frac{\beta\omega_n}{2} \quad (9)$$

For two specific frequencies  $\omega_n$  and  $\omega_m$ , and the related damping ratio  $\zeta_n$  and  $\zeta_m$ , the Rayleigh damping coefficient and  $\alpha$  and  $\beta$  can be obtained by solving a pair of simultaneous equations.

Rewriting Equation (9) then gives:

$$\begin{bmatrix} \zeta_m \\ \zeta_n \end{bmatrix} = \frac{1}{2} \begin{bmatrix} 1/\omega_m & \omega_m \\ 1/\omega_n & \omega_n \end{bmatrix} \begin{bmatrix} \alpha \\ \beta \end{bmatrix} \quad (10)$$

After solving simultaneously, the following equation is obtained:

$$\begin{bmatrix} \alpha \\ \beta \end{bmatrix} = 2 \frac{\omega_m\omega_n}{\omega_n^2 - \omega_m^2} \begin{bmatrix} \omega_n & -\omega_m \\ -1/\omega_n & 1/\omega_n \end{bmatrix} \begin{bmatrix} \zeta_m \\ \zeta_n \end{bmatrix} \quad (11)$$

It is usually assumed that the sum of  $\alpha$  and  $\beta$  is approximately constant over a frequency range to obtain a given damping ratio  $\zeta$ . Therefore, when the damping ratio  $\zeta$  and the frequency interval  $\omega_1 - \omega_2$  are given,  $\alpha$  and  $\beta$  are calculated by:

$$\alpha = 2\zeta \frac{\omega_1\omega_2}{\omega_1 + \omega_2} \quad (12)$$

$$\beta = \frac{2\xi}{\omega_1 + \omega_2} \quad (13)$$

### 2.1. Rayleigh Damping in Implicit Calculations

In the implicit method, the new value given for a given step size contains one or more values related to this step, so the required amount of trial values must be assumed and then improved through successive iterations.

A general numerical approach to step-by-step dynamic reactions is to apply an integral forward step from the initial to final conditions for each time step. Its basic concept can be expressed by the following formula [37]:

$$\dot{u}_{t+\Delta t} = \dot{u}_t + \int_t^{t+\Delta t} \ddot{u}(\tau) d\tau \quad (14)$$

$$u_{t+\Delta t} = u_t + \int_t^{t+\Delta t} \dot{u}(\tau) d\tau \quad (15)$$

This represents the final velocity and displacement in terms of the initial values of these values plus an integral expression.

Take *Newmark* –  $\beta$ , which often appears in implicit calculations, as an example. *Newmark* –  $\beta$  makes the following assumptions about the basic integral of the above formula [37]:

$$\dot{u}_{t+\Delta t} = \dot{u}_t + (1 - \gamma)\Delta t \ddot{u}_t + \gamma\Delta t \ddot{u}_{t+\Delta t} \quad (16)$$

$$u_{t+\Delta t} = u_t + \Delta t \dot{u}_t + \left(\frac{1}{2} - \delta\right) \Delta t^2 \ddot{u}_t + \delta \Delta t^2 \ddot{u}_{t+\Delta t} \quad (17)$$

The coefficient  $\gamma$  provides the weight of the linear change between the contribution of the initial and final acceleration to the velocity change, and the coefficient  $\beta$  provides the weight of the contribution of the initial and final acceleration to the displacement change.

Bringing this into the dynamic equation gives [37]:

$$(K + a_0M + a_1C)u_{t+\Delta t} = P_{t+\Delta t} + (a_0u_t + a_2\dot{u}_t + a_3\ddot{u}_t)M + (a_1u_t + a_4\dot{u}_t + a_5\ddot{u}_t)C \quad (18)$$

In the above formula:  $a_0 = \frac{1}{\delta\Delta t^2}$ ,  $a_1 = \frac{\gamma}{\delta\Delta t}$ ,  $a_2 = \frac{1}{\delta\Delta t}$ ,  $a_3 = \frac{1}{2\delta} - 1$ ,  $a_4 = \frac{\gamma}{\delta} - 1$ , and  $a_5 = \frac{\gamma - 2\delta}{2\delta} \Delta t$ .

Substituting into Equation (8) gives [37]:

$$\begin{aligned} & \{(1 + \beta)K + (a_0 + \alpha a_1)M\}u_{t+\Delta t} = P_{t+\Delta t} \\ & + \{(a_0 + \alpha a_1)u_t + (a_2 + \alpha a_4)\dot{u}_t + (a_3 + \alpha a_5)\ddot{u}_t\}M + \beta(a_1u_t + a_4\dot{u}_t + a_5\ddot{u}_t)K \end{aligned} \quad (19)$$

In the implicit calculation, Rayleigh damping is fully included in the formula, and mass damping  $\alpha$  and stiffness damping  $\beta$  can be directly input. The same is true for another common Wilson method.

### 2.2. Rayleigh Damping in Explicit Calculations

In explicit algorithms, new reaction values calculated at each step depend only on quantities already obtained in previous steps. The most representative one is the central difference method, whose basic assumptions are [37]:

$$\ddot{u}_t = \frac{1}{\Delta t}(u_{t-\Delta t} - 2u_t + u_{t+\Delta t}) \quad (20)$$

$$\dot{u}_{t+\Delta t} = \frac{1}{2\Delta t}(-u_{t-\Delta t} + u_{t+\Delta t}) \quad (21)$$

Bringing this into the dynamic equation gives [37]:

$$\left(\frac{1}{\Delta t^2}M + \frac{1}{2\Delta t}C\right)u_{t+\Delta t} = P_{t+\Delta t} - \left(K - \frac{2}{\Delta t^2}M\right)u_t - \left(\frac{1}{\Delta t^2}M - \frac{1}{2\Delta t}C\right)u_{t-\Delta t} \quad (22)$$

We find that the coefficients before the new reaction values do not contain the stiffness matrix, and if  $M$  and  $C$  are diagonal matrices, then solving the equation will not require a solution matrix. However, if Rayleigh damping is used, then substituting into Equation (19) gives [37]:

$$\left(\left(\frac{1}{\Delta t^2} + 2\alpha\frac{1}{2\Delta t}\right)M + 2\beta\frac{1}{2\Delta t}K\right)u_{t+\Delta t} = P_{t+\Delta t} - \left(K - \frac{2}{\Delta t^2}M\right)u_t - \left(\frac{1}{\Delta t^2}M - \frac{1}{2\Delta t}C\right)u_{t-\Delta t} \quad (23)$$

Obviously, the coefficients will contain the stiffness matrix  $K$ , which means that the matrix needs to be solved. Due to the step size of the displayed calculation, the calculation speed will become extremely slow. Therefore, Rayleigh damping is generally not used directly for display integration, but ignoring the stiffness matrix will cause high-order vibration shapes or high-frequency components in seismic waves to participate in the vibration too much, distorting the simulation results.

### 3. Model Introduction

#### 3.1. AP1000 Nuclear Power Plant

The whole AP1000 NPP is composed of a reinforced concrete shield building (RCSB), steel vessel containment (SVC), and reinforced concrete auxiliary building (RCAB). The thickness of the shear wall of the containment building is 91.4 cm, and the thickness of the steel plate in the steel containment building is 4.8 cm. The auxiliary factory building has 7 floors, and the thickness of the floor slab and shear wall are 23 cm and 60 cm, respectively. The geometric dimensions of the AP1000 nuclear power plant are shown in Figure 1, and the material parameters are shown in Table 1.

The whole AP1000 NPP was established by ANSYS/LS-DYNA and modeled using an explicit thin structural shell element (SHELL163) with many formulations. Among the formulations of SHELL163, the Belytschko–Tsay shell element was adopted in this study owing to its speed. The rebar was modeled using a beam element (BEAM161) with the Hughes–Liu integral algorithm. SHELL163 and BEAM161 were connected via common nodes to model the reinforced concrete. The mesh size was 2 m × 2 m [38]. Furthermore, because the structure of the whole AP1000 NPP was too complex, the internal equipment in the AP1000 NPP was simulated by equivalent members according to the literature [39]. Information about the shape functions of SHELL163 and BEAM161 can be found in Ref. [40].

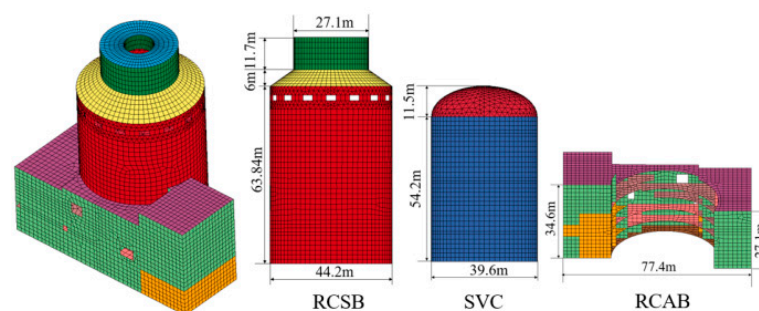


Figure 1. Model of AP1000 nuclear power plant.

Table 1. AP1000 nuclear power plant material parameters.

Material	Concrete	Steel Plate and Rebar	Foundation
Density (kg/m <sup>3</sup> )	2300	7800	2500
Elastic modulus (MPa)	$3.35 \times 10^4$	$2.06 \times 10^5$	$1.463 \times 10^5$
Poisson's ratio	0.2	0.3	0.3

### 3.2. Soil-Structure Interaction System

According to the requirements of nuclear power codes [41,42], the interaction between the foundation and the superstructure should be considered in the dynamic analysis calculation of nuclear power structures, and the foundation grid size should meet the following requirements [43]:

$$L_m < \frac{V_s}{af_n} \quad (24)$$

In the above formula,  $L_m$  is the maximum grid size in the foundation,  $V_s$  is the shear wave speed of the foundation,  $f_n$  is the Nyquist frequency, and  $a$  is a constant between 5 and 10. The shear wave speed of the foundation material was 1067 m/s, the shear modulus was 2.845 GPa, the density was 2500 kg/m<sup>3</sup>, and the Poisson's ratio was 0.2 [39,44]. Therefore, the foundation grids were all less than 6 m. Based on the literature [43,44], the foundation size was taken as 220 m × 200 m × 40 m.

A perfectly matched layer [45] was employed in explicit calculations to simulate open and reflection-free infinite domains. In the implicit integration, a viscoelastic boundary [46] was used to simulate the semi-infinite space of the foundation. The finite element models for explicit and implicit calculations are shown in Figures 2 and 3. The number of elements and nodes in the two finite element models were the same, and are listed in Table 2.

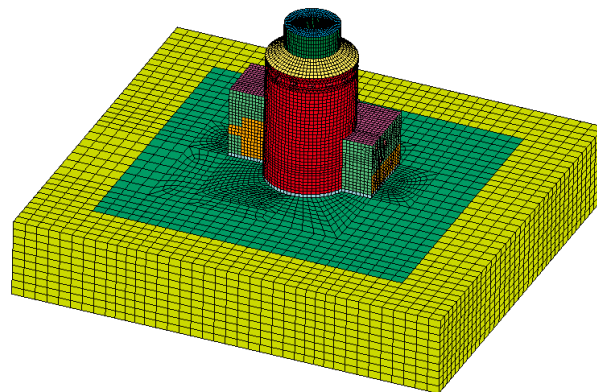


**Figure 2.** The finite element models for explicit calculations.

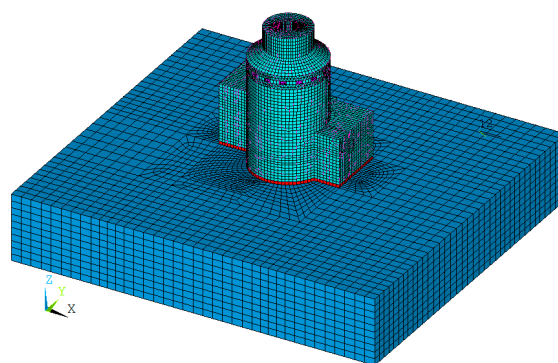


**Figure 3.** The finite element models for implicit calculations.

**Table 2.** The numbers of elements and nodes in the SSI system.

	Mesh Size	Number of Elements	Number of Nodes
Whole NPPs	2 m × 2 m	19,863	16,797
Soil foundation	Less than 5 m	36,010	39,490

### 3.3. Model Validation

The unit type and integration method of the overall soil–structure interaction model in explicit calculation and implicit calculation are different. To ensure the rationality of the two models, the comparison of the first five-order natural frequencies is shown in Table 3. The relative error of the fundamental frequency of the two models is  $-0.358\%$ , and the maximum relative error of the first five natural frequencies is  $4.525\%$ , both of which are less than  $5\%$ . Within a reasonable range, this shows that the finite element model used by the two different integration methods had better consistency.

Although the settings of the two models were as consistent as possible, there were still slight differences between the two models due to the differences in element types and integration methods in explicit and implicit integration. In the implicit integration model, the difference between the third and fourth modes was very small, possibly due to the fourth mode being the mode of an internal component rather than the mode of the overall model. Therefore, the fourth mode of the two models had a significant difference, and the fifth mode of the implicit integration model was very close to the fourth mode of the explicit integration model.

**Table 3.** Comparison of self-oscillation frequencies.

Mode	Natural Frequency (Implicit) (Hz)	Natural Frequency (Explicit) (Hz)	Relative Error (%)
1	2.791	2.781	$-0.358$
2	2.984	2.983	$-0.034$
3	4.033	4.085	1.289
4	4.088	4.273	4.525
5	4.228	4.363	3.193

### 3.4. Input Ground Motions

As shown in Figure 4, the benchmark input ground motion was an artificial wave fitted to the Rg1.60 response spectrum with a  $5\%$  damping ratio. The horizontal and vertical peak values were both  $0.3\text{ g}$ . The ground motion input position was defined at the upper surface of the foundation. The ground motion lasted for  $30\text{ s}$ , and the step size was  $0.01\text{ s}$  long.

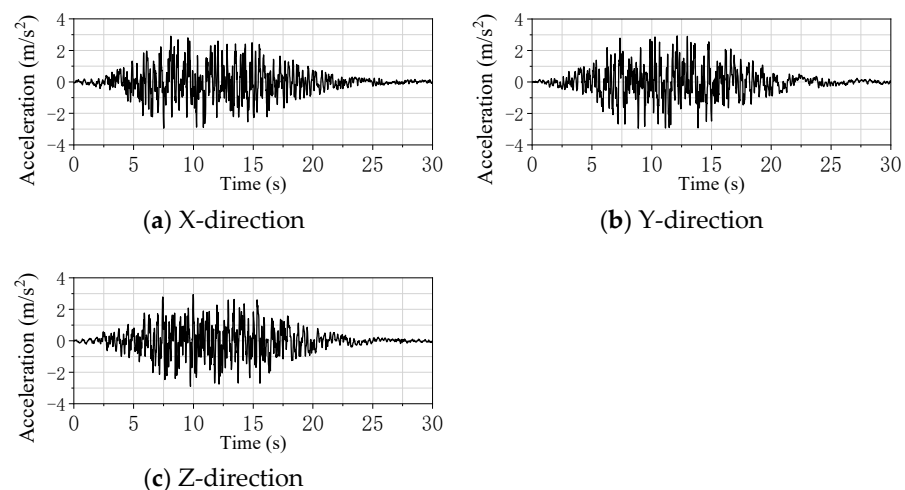


**Figure 4.** Inputting ground motions.

## 4. Rayleigh Damping Parameter Calculation

It can be seen from Table 3 that the natural frequency of the finite element model in the implicit calculation was  $2.791\text{ Hz}$ , and the natural frequency of the finite element model in the explicit calculation was  $2.781\text{ Hz}$ . The relative error between the two was only  $-0.358\%$ . In the calculation of Rayleigh damping, the natural frequency of the model was uniformly

taken as 2.791 Hz. The energy of seismic waves is mostly concentrated within 15 Hz, so this value was taken as 15 Hz. If the structural damping ratio is 5%, then the Rayleigh damping coefficient in the implicit calculation can be obtained from Equations (12) and (13).

The mass damping in explicit calculations can be written as:

$$\alpha_{dyna} = \frac{4\zeta\pi}{T} = 2\zeta\omega \quad (25)$$

where  $T = \frac{2\pi}{\omega}$ ,  $T$  is the natural vibration period of the structure, and  $\omega$  is the natural vibration frequency of the structure.

LS-DYNA provides two methods for calculating stiffness damping in explicit calculations.

When the damping coefficient value is less than 0, the old, alternative stiffness damping formula is used, in which the coefficient value is approximately equal to the  $\beta$  value in Rayleigh damping, as shown below:

$$-COEF = \beta_{dyna} = \frac{2\zeta}{\omega} \quad (26)$$

This old stiffness damping formula is particularly prone to instability in numerical calculations.

When the damping coefficient takes a value greater than 0, stiffness damping provides an approximate fraction of the critical damping in the high frequency domain. For example,  $COEF = 0.1$  is approximately 10% of critical damping.

Based on the above discussion, comparative research based on the work cases in Table 4 was performed.

**Table 4.** The work cases.

Work Cases	Damping-Part-Mass	Damping-Part-Stiffness
Case 1 (NPSSI)	1.479	$8.946 \times 10^{-4}$
Case 2 (LS-DYNA)	1.479	$8.946 \times 10^{-4}$
Case 3 (LS-DYNA)	1.479	$-8.946 \times 10^{-4}$
Case 4 (LS-DYNA)	1.754	$-8.946 \times 10^{-4}$
Case 5 (LS-DYNA)	1.754	0.05

Note: In LS-DYNA, when the stiffness damping is set to  $-5.702 \times 10^{-3}$ , the calculation will become unstable and cannot be calculated.

## 5. Results and Analysis

Node A, located at the top of the RCSB, and node B, located at the center of the bottom raft, were selected. The locations of the two nodes are shown in Figure 5. The X-directional displacement time history of node A and node B under different working cases are shown in Figures 6 and 7. At the same time, the spectral acceleration of the two nodes in the X-direction were compared, as shown in Figures 8 and 9. The frequency points of the response spectrum were selected according to the suggested frequency intervals given by the standards for the seismic design of nuclear power plants [47], which are shown in Table 5.

**Table 5.** Suggested frequency intervals for calculation of response spectra [47].

Frequency Range (Hz)	Increment (Hz)
0.2–3.0	0.10
3.0–3.6	0.15
3.6–5.0	0.20
5.0–8.0	0.25
8.0–15.0	0.50
15.0–18.0	1.0
18.0–22.0	2.0
22.0–33	3.0

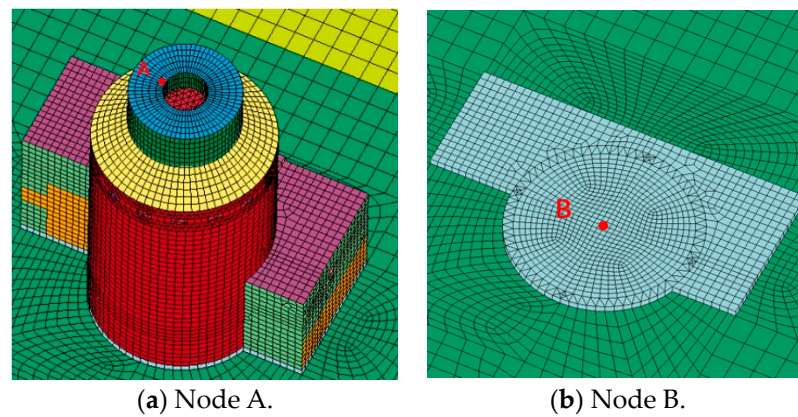


Figure 5. Schematic diagram of node A and node B locations.

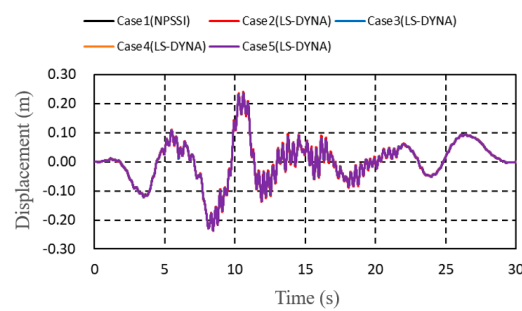


Figure 6. The X-directional displacement time history of node A.

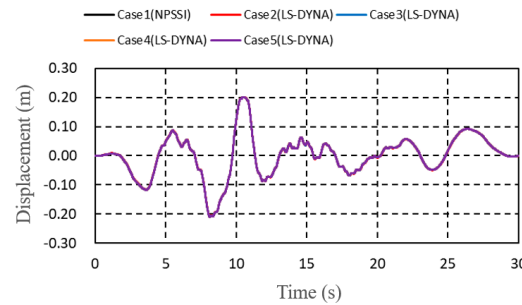


Figure 7. The X-directional displacement time history of node B.

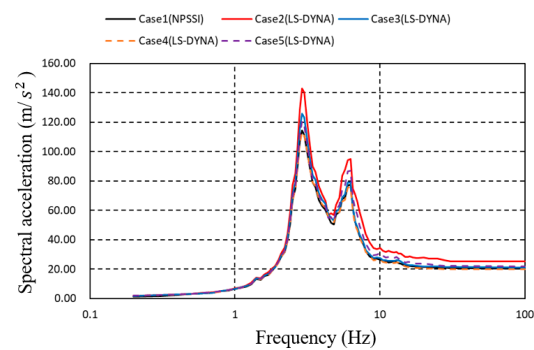
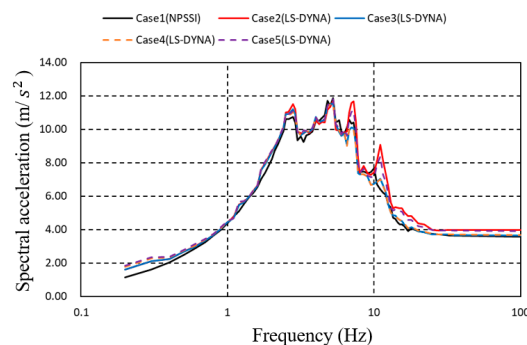


Figure 8. The X-directional spectral acceleration of node A.



**Figure 9.** The X-directional spectral acceleration of node B.

From Figures 6 and 7, it can be seen that the different values of the Rayleigh damping parameter in the explicit integral had a more significant impact on the structural acceleration than displacement. The displacement time history curves of different working cases in Figure 7 almost overlap. As shown in Figures 8 and 9, the different values of Rayleigh damping parameter in the explicit integral had a great influence on the peak values of spectral acceleration, but the frequency corresponding to the peak spectral acceleration remained almost unchanged.

In order to assess the accuracy of different cases, the comparison of the peak values of spectral acceleration between Case 1 and the other cases are shown in Tables 6 and 7. It can be observed that the results of Case 3 and Case 4 were similar to those in implicit dynamic analysis.

**Table 6.** The comparison of peak values of the spectral acceleration of node A.

Frequency (Hz)	Case 1 (m/s <sup>2</sup> )	Case 2		Case 3		Case 4		Case 5	
		Value (m/s <sup>2</sup> )	Relative Error (%)	Value (m/s <sup>2</sup> )	Relative Error (%)	Value (m/s <sup>2</sup> )	Relative Error (%)	Value (m/s <sup>2</sup> )	Relative Error (%)
3.00	111.45	140.30	25.88	123.40	10.72	110.80	−0.58	117.50	5.43
6.25	77.60	94.84	22.22	79.04	1.86	75.44	−2.78	86.96	12.07

**Table 7.** The comparison of peak values of spectral acceleration of node B.

Frequency (Hz)	Case 1 (m/s <sup>2</sup> )	Case 2		Case 3		Case 4		Case 5	
		Value (m/s <sup>2</sup> )	Relative Error (%)	Value (m/s <sup>2</sup> )	Relative Error (%)	Value (m/s <sup>2</sup> )	Relative Error (%)	Value (m/s <sup>2</sup> )	Relative Error (%)
2.80	10.76	11.52	7.07	11.21	4.19	11.06	2.79	11.12	3.35
5.25	11.88	11.70	−1.52	11.59	−2.44	11.50	−3.20	11.81	−0.59
7.25	10.40	11.68	12.32	10.08	−3.07	9.98	−4.05	11.12	6.93
11.00	6.40	9.07	41.80	7.03	9.97	7.00	9.47	8.39	31.22

## 6. Conclusions

Based on the calculation method of the Rayleigh damping coefficient in implicit integration and the results of the implicit dynamic analysis, this paper studied the influence of different calculation methods of the Rayleigh damping coefficient in explicit integration on the dynamic response of the structure. The following conclusions were drawn:

- (1) The results show that in explicit calculations, different calculation methods of Rayleigh damping and the value of the damping coefficient have a greater impact on the dynamic response of the nuclear power structure.
- (2) The mass component of Rayleigh damping mainly affects the low-frequency response of the structure, and the stiffness component mainly affects the high-frequency response of the structure.

- (3) In order to obtain results for explicit and implicit dynamic analysis with good consistency, the Rayleigh damping mass component should be obtained by Equation (25) or taken as the same value as the implicit integral, and the stiffness component of the Rayleigh damping in the explicit integral should be taken as the negative number of the stiffness component in the implicit integral.

**Author Contributions:** Methodology, Y.C.; Software, Y.C.; Formal analysis, H.W. and M.C.; Investigation, Y.W. and P.X.; Resources, Z.B. and J.L.; Writing—original draft, H.W. and Z.B.; Writing—review and editing, Y.C.; Supervision, J.Z.; Funding acquisition, J.L. All authors have read and agreed to the published version of the manuscript.

**Funding:** This work has been supported by the National S&T Major Project (Grant No. ZX069), Grant 52178460 from the National Natural Science Foundation of China.

**Data Availability Statement:** All the data used has been included in the article.

**Conflicts of Interest:** Authors Yan Chen, Yougang Wang, Junhong Zhang and Zitong Bao were employed by the company China National Nuclear Corporation (CNNC). The remaining authors declare that the research was conducted in the absence of any commercial or financial relationships that could be construed as a potential conflict of interest.

## References

1. Idriss, I.M.; Lysmer, J.; Hwang, R.N.; Seed, H.B. *QUAD4: A Computer Program for Evaluating the Seismic Response of Soil Structures by Variable Damping Finite Element Procedures*; University of California: Berkeley, CA, USA, 1973.
2. Hu, C.; Wang, Y.; Ling, D. Physical essence and influence of model parameters on dynamic response of Rayleigh damping. *J. Zhejiang Univ. (Eng. Sci.)* **2017**, *51*, 1284–1290. (In Chinese)
3. Yoshida, N.; Kobayashi, S.; Suetomi, I.; Miura, K. Equivalent linear method considering frequency dependent characteristics of stiffness and damping. *Soil Dyn. Earthq. Eng.* **2002**, *22*, 205–222. [[CrossRef](#)]
4. Yu, T.; Shao, L. Calculation and Application of Rayleigh Damping Coefficient for Dynamic Response Analysis of Extra-thick Overburden. *Hydropower Pumped Storage* **2020**, *6*, 33–39+73. (In Chinese)
5. Wang, T.; Ding, J.; Lou, M. Discussion on the methods of estimating structural vibration from railway lines and the determination of damping matrix. *J. Vib. Shock* **2008**, *11*, 77–79+100+200. (In Chinese) [[CrossRef](#)]
6. Lou, M.; Sui, L.; Shen, F. Effects of Damping Matrix Modeling on Seismic Responses of Super High-rise Structures. *Struct. Eng.* **2013**, *29*, 55–61. (In Chinese) [[CrossRef](#)]
7. Lou, M.; Shao, X. Coefficient Selection of Damping Matrix in Explicit Calculation of Soil Layer Seismic Response. *J. Tongji Univ. (Nat. Sci.)* **2013**, *41*, 1126–1132. (In Chinese)
8. Lou, M.; Yin, L.; Shao, X. Discussions on numerical simulation problem of damping matrix of high-rise earth-rock filled dam seismic response analysis in time domain. *Earthquake Eng. Eng. Dyn.* **2018**, *38*, 33–42. (In Chinese) [[CrossRef](#)]
9. Pan, D. An Optimization Method for the Direct Determination of Rayleigh Damping Coefficients. *Eng. Mech.* **2013**, *30*, 16–21. (In Chinese)
10. Pan, D. An Optimization Solution for Rayleigh Damping Coefficients in Seismic Response Analysis. *Eng. Mech.* **2013**, *30*, 15–20+27. (In Chinese)
11. Pan, D.; Cheng, Y.; Li, X. Comparison study on Rayleigh damping construction methods for long-span reticulated shell seismic response. *J. Harbin Inst. Technol.* **2017**, *49*, 45–52. (In Chinese)
12. Cheng, Y.; Pan, D. An optimization solution for equivalent Rayleigh damping for site seismic response under hysteretic damping. *Rock Soil Mech.* **2021**, *42*, 2023–2030+2040. (In Chinese) [[CrossRef](#)]
13. Yang, D.B.; Zhang, Y.G.; Wu, J.Z. Computation of Rayleigh damping coefficients in seismic time-history analysis of spatial structures. *J. Int. Assoc. Shell Spat. Struct.* **2010**, *51*, 125–135.
14. Zhu, X.; Liu, Z.; Pan, R.; Hou, C.; Gong, Y. Analysis of the influence of different methods for determining Rayleigh damping coefficient on non-rock site seismic response. *Ind. Constr.* **2015**, *45*, 31–36. (In Chinese)
15. Zou, D.; Xu, B.; Kong, X. Study of influence of different methods for calculating Rayleigh damping coefficient on high earth-rock dam seismic response. *Rock Soil Mech.* **2011**, *32*, 797–803. (In Chinese) [[CrossRef](#)]
16. Li, Z.; Wu, S. Calculation Method and Experimental Study of Rayleigh Damping Coefficients of Quayside Container Cranes in Normal Conditions. *China Earthq. Eng. J.* **2020**, *42*, 1417–1426. (In Chinese)
17. Xu, Z.; Du, X.; Xu, C.; Zhang, C.; Jiang, J. Comparison of determination methods of site Rayleigh damping coefficients in seismic response analysis of underground structures. *Rock Soil Mech.* **2019**, *40*, 4838–4847. (In Chinese)
18. Shi, Y.; Lin, S.; Zhao, H. Influence of Rayleigh damping parameters on site response under action of Rayleigh wave. *Yangtze River* **2017**, *48*, 75–80. (In Chinese)
19. Tang, Y.; Lou, M.; Luo, C.; Liu, H.; Yin, L. Discussion on Rayleigh Damping Matrix Modeling of High-rise Arch Dam Seismic Response Analysis in Time Domain. *J. Disaster Prev. Mitig. Eng.* **2023**, *43*, 518–525. (In Chinese) [[CrossRef](#)]

20. Haukaas, T. Exact Sensitivity of Nonlinear Dynamic Response with Modal and Rayleigh Damping Formulated with the Tangent Stiffness. *J. Struct. Eng.* **2024**, *150*, 04024012. [[CrossRef](#)]
21. Li, S.; Brun, M.; Gravouil, A.; Fekak, F.E. Explicit/implicit multi-time step simulation of bridge crane under earthquake with frictional contacts and high-frequency Rayleigh damping. *Finite Elem. Anal. Des.* **2023**, *220*, 103946. [[CrossRef](#)]
22. Jing, Z.; Ruixiang, S.; Yubin, W.; Bideng, L.; Lei, H.; Qiong, W. Study on the Influence of Rayleigh Damping Coefficient on the Subway Vibration Response of Building Structures. In Proceedings of the International Congress on Sound and Vibration, Prague, Czech Republic, 31 January 2023.
23. Huang, J.; Li, X.; Zhang, J.; Sun, Y.; Ren, J. Determining the Rayleigh damping parameters of flexible pavements for finite element modeling. *J. Vib. Control* **2022**, *28*, 3181–3194. [[CrossRef](#)]
24. Jimenez, G.A.L.; Dias, D.; Jenck, O. Seismic loading response of piled systems on soft soils-Influence of the Rayleigh damping. *Geomech. Eng.* **2022**, *29*, 155–170.
25. Rahul, B.; Dharani, J.; Balaji, R. Optimal method for determination of rayleigh damping coefficients for different materials using modal analysis. *Int. J. Veh. Struct. Syst.* **2021**, *13*, 102–111.
26. Matveyenko, V.P.; Kligman, E.P. Natural Vibration Problem of Viscoelastic Solids as Applied to Optimization of Dissipative Properties of Constructions. *J. Vib. Control.* **1997**, *3*, 87–102. [[CrossRef](#)]
27. Beytullah, T. Transient analysis of viscoelastic helical rods subject to time-dependent loads. *Int. J. Solids Struct.* **2004**, *41*, 1605–1624.
28. Khudainazarov, S.; Sabirjanov, T.; Ishmatov, A. Assessment of Dynamic Characteristics of High-Rise Structures Taking into Account Dissipative Properties of the Material. *J. Phys. Conf. Ser.* **2019**, *1425*, 012009. [[CrossRef](#)]
29. Temel, B.; Aslan, T.A.; Noori, A.R. In-plane vibration analysis of parabolic arches having a variable thickness. *Int. J. Dyn. Control* **2021**, *9*, 910–921. [[CrossRef](#)]
30. Noori, A.R.; Aslan, T.A.; Temel, B. Dynamic Analysis of Functionally Graded Porous Beams Using Complementary Functions Method in the Laplace Domain. *Compos. Struct.* **2021**, *256*, 113094. [[CrossRef](#)]
31. Cao, J.; Bu, F.; Wang, J.; Bao, C.; Chen, W.; Dai, K. Reconstruction of full-field dynamic responses for large-scale structures using optimal sensor placement. *J. Sound Vib.* **2023**, *554*, 117693. [[CrossRef](#)]
32. Guo, X.; Ding, C.; Wei, P.; Yang, R. Theoretical analysis of the interaction between blasting stress wave and linear interface crack under high in-situ stress in deep rock mass. *Int. J. Rock Mech. Min. Sci.* **2024**, *176*, 105723. [[CrossRef](#)]
33. Deng, E.-F.; Wang, Y.-H.; Zong, L.; Zhang, Z.; Zhang, J.-F. Seismic behavior of a novel liftable connection for modular steel buildings: Experimental and numerical studies. *Thin-Walled Struct.* **2024**, *197*, 111563. [[CrossRef](#)]
34. Xie, J. Discussion on damping in structural seismic response analysis. *Build. Struct.* **2015**, *45*, 53–58. (In Chinese)
35. Wolf, J.P. *Dynamic Soil-Structure Interaction*; Prentice-Hall, Inc.: Englewood Cliffs, NJ, USA, 1985.
36. Hudson, M.; Idriss, I.M.; Beikae, M. *QUAD4M: A Computer Program to Evaluate the Seismic Response of Soil Structures Using Finite Element Procedures and Incorporating a Compliant Base*; Center for Geotechnical Modeling, Department of Civil and Environmental Engineering, University of California: Berkeley, CA, USA, 1994.
37. Clough, R.; Penzien, J. *Dynamics of Structures*; Computers and Structures, Inc.: Berkeley, CA, USA, 2003.
38. Xu, Q.; Chen, J.; Zhang, C.; Li, J.; Zhao, C. Dynamic analysis of AP1000 shield building considering fluid and structure interaction effects. *Nucl. Eng. Technol.* **2016**, *48*, 246–258. [[CrossRef](#)]
39. AP1000 Design Control Document (DCD). Tier 2, Chapter 3. In *Design of Structures, Components, Equipment and Systems, Revision 15*; Westinghouse Electric Company LLC.: Cranberry, PA, USA, 2011.
40. Hallquist, J.O. *LS-DYNA Theory Manual*; Livermore Software Technology Corporation: Livermore, CA, USA, 2006.
41. *SRP 3.7.1*; Standard Review Plan-Seismic Design Parameters. SRP 3.7.1. U.S. Nuclear Regulatory Commission: Washington, DC, USA, 2014.
42. *Asce4-16*; Seismic Analysis of Safety-Related Nuclear Structures. American Society of Civil Engineers: Reston, VA, USA, 2016.
43. Sextos, A.G.; Manolis, G.D.; Athanasiou, A. Seismically induced uplift effects on nuclear power plants. Part 1: Containment building rocking spectra. *Nucl. Eng. Des.* **2017**, *318*, 276–287. [[CrossRef](#)]
44. Li, J.; Mei, R.; Wang, Y. Vibration analysis of third generation nuclear power plant considering soil-structure-interaction effect under the impact of large commercial aircraft. *Struct. Des. Tall Spec. Build.* **2020**, *29*, e1796. [[CrossRef](#)]
45. Bermúdez, A.; Hervella-Nieto, L.; Prieto, A. An optimal perfectly matched layer with unbounded absorbing function for time-harmonic acoustic scattering problems. *J. Comput. Phys.* **2007**, *223*, 469–488. [[CrossRef](#)]
46. Zhou, C. Research on the Mechanism of Seismic Wave Input about High Rockfill Dam. Master’s Thesis, Dalian University of Technology, Dalian, China, 2009. (In Chinese)
47. *GB50267-2019*; Standard for Seismic Design of Nuclear Power Plants. Ministry of Housing and Urban-Rural Development of the People’s Republic of China: Beijing, China, 2019.

**Disclaimer/Publisher’s Note:** The statements, opinions and data contained in all publications are solely those of the individual author(s) and contributor(s) and not of MDPI and/or the editor(s). MDPI and/or the editor(s) disclaim responsibility for any injury to people or property resulting from any ideas, methods, instructions or products referred to in the content.